frontiers | Frontiers in Chemistry

ORIGINAL RESEARCH
published: 18 May 2022
doi: 10.3389/fchem.2022.845617

In Situ Formation of Bi_2MoO_6-Bi_2S_3 Heterostructure: A Proof-Of-Concept Study for Photoelectrochemical Bioassay of L-Cysteine

Hui-Jin Xiao [1], Xiao-Jing Liao [1], Hui Wang [1], Shu-Wei Ren [2], Jun-Tao Cao [1] and Yan-Ming Liu [1]**

[1]Xinyang Key Laboratory of Functional Nanomaterials for Bioanalysis, College of Chemistry and Chemical Engineering, Xinyang Normal University, Xinyang, China, [2]Xinyang Central Hospital, Xinyang, China

A novel signal-increased photoelectrochemical (PEC) biosensor for L-cysteine (L-Cys) was proposed based on the Bi_2MoO_6–Bi_2S_3 heterostructure formed *in situ* on the indium–tin oxide (ITO) electrode. To fabricate the PEC biosensor, Bi_2MoO_6 nanoparticles were prepared by a hydrothermal method and coated on a bare ITO electrode. When L-Cys existed, Bi_2S_3 was formed *in situ* on the interface of the Bi_2MoO_6/ITO electrode by a chemical displacement reaction. Under the visible light irradiation, the Bi_2MoO_6–Bi_2S_3/ITO electrode exhibited evident enhancement in photocurrent response compared with the Bi_2MoO_6/ITO electrode, owing to the signal-increased sensing system and the excellent property of the formed Bi_2MoO_6–Bi_2S_3 heterostructure such as the widened light absorption range and efficient separation of photo-induced electron–hole pairs. Under the optimal conditions, the sensor for L-Cys detection has a linear range from 5.0×10^{-11} to 1.0×10^{-4} mol L^{-1} and a detection limit of 5.0×10^{-12} mol L^{-1}. The recoveries ranging from 90.0% to 110.0% for determining L-Cys in human serum samples validated the applicability of the biosensor. This strategy not only provides a method for L-Cys detection but also broadens the application of the PEC bioanalysis based on *in situ* formation of photoactive materials.

Keywords: photoelectrochemical sensor, Bi_2MoO_6–Bi_2S_3 heterostructure, L-cysteine, *in situ* formation reaction, ion exchange reaction

OPEN ACCESS

Edited by:
Junjie Zhu,
Nanjing University, China

Reviewed by:
Jing Qian,
Jiangsu University, China
Wei Chen,
Fujian Medical University, China

***Correspondence:**
Jun-Tao Cao
jtcao11@163.com
Yan-Ming Liu
liuym9518@sina.com

Specialty section:
This article was submitted to Analytical Chemistry, a section of the journal Frontiers in Chemistry

Received: *30 December 2021*
Accepted: *24 March 2022*
Published: *18 May 2022*

Citation:
Xiao H-J, Liao X-J, Wang H, Ren S-W, Cao J-T and Liu Y-M (2022) In Situ Formation of Bi_2MoO_6-Bi_2S_3 Heterostructure: A Proof-Of-Concept Study for Photoelectrochemical Bioassay of L-Cysteine. Front. Chem. 10:845617. doi: 10.3389/fchem.2022.845617

INTRODUCTION

L-Cysteine (L-Cys), which is involved in the process of protein synthesis, affects the function of protein and plays an important role in the life system (Palego et al., 2015). Its abnormal levels in human serum are associated with lots of diseases, and thus it is considered a significant biomarker. For instance, people with heart disease and liver injury often have low levels of L-Cys in their blood (Wu et al., 2016), whereas people with Alzheimer's disease and cancer often have high levels of L-Cys (Li et al., 2014b; Huang et al., 2018). Therefore, monitoring the content of L-Cys in human body is meaningful. Currently, some analytical methods such as high-performance liquid chromatography (Deáková et al., 2015), mass spectrometry (Li et al., 2014a), fluorescence (Li et al., 2019), colorimetry (Song et al., 2018), and photoelectrochemistry (PEC) (Peng et al., 2020) have been developed for L-Cys detection.

PEC analysis, a fast, efficient, and low background analytical method, has attracted great attention in recent years (Cao et al., 2021; Lv et al., 2021; Zhu et al., 2021). Until now, many sensing principles

have been exploited and adopted for the PEC bioanalysis, such as steric hindrance effect (Wang et al., 2019c; Meng et al., 2020), electron donor/acceptor reaction (Li et al., 2017; Wang et al., 2019b), exciton–plasmon interactions (Ma et al., 2016; Dong et al., 2017), plasmon-enhanced effect (Li et al., 2016; Qiu et al., 2018), and *in situ* growth reaction (Qiu and Tang, 2020). Of these, the signaling mechanism based on the *in situ* growth reaction that acts directly on the electrode is not only simple to operate but also with a low background signal (Hou et al., 2016). For example, on the basis of the reaction between L-Cys and copper compounds, Zhu et al. (2017) constructed a PEC bioassay of L-Cys using a CuO–Cu_2O heterojunction as a photoactive material. By using the reaction between Cu^{2+} and S^{2-} from the WO_3–Au–CdS nanocomposite, Zhang et al. (2019) designed a PEC immunoassay for the prostate-specific antigen. However, these works have always quantified the targets based on the signal decrease, which limits the sensitivity to some extent. By the reaction between Ag^+ and BiOI/Ni electrode, Yu et al. (2019a) constructed a signal-increased biosensing system. In this system, the AgI–Ag–BiOI Z-scheme heterojunction formed *in situ* greatly enhanced the PEC response, achieving satisfied detection sensitivity and stability. Considering the good performance and the few reports of such strategy, exploiting the new *in situ* growth reaction to construct signal-increased sensing systems and extending their applications in PEC bioanalysis are urgent and necessary.

Among various semiconductor materials, bismuth-based semiconductors possess advantages of good biocompatibility and highly visible light response (Chen et al., 2016; Zhou et al., 2017; Yu et al., 2019b). Bi_2MoO_6, featuring non-toxic, good stability, and adjustable morphology (Li et al., 2020), has attracted wide attention. In addition, Bi_2MoO_6 has a layered structure with a $[Bi_2O_2]^{2+}$ layer stuck between two MoO_4^{2-} slabs, which makes it have lots of active surfaces (Wu et al., 2018), while the PEC performance of Bi_2MoO_6 leaves much to be desired due to the rapid recombination between holes and electrons. In order to restrain such recombination, constructing heterostructures is one of the most effective strategies (Wang et al., 2019a; Liao et al., 2021). As a method to form heterojunctions, ion exchange can be excited by the differences in solubility of different substances and helps maintain their original state to a large extent (Wang et al., 2017). Intelligently, both Bi_2MoO_6 and Bi_2S_3 contain bismuth element, and the solubility of Bi_2S_3 is far less than that of Bi_2MoO_6. Based on this, whether the principle of the ion exchange reaction can be used for *in situ* generation of Bi_2MoO_6–Bi_2S_3 heterostructure and construction of a PEC biosensor?

A signal-increased PEC biosensor for L-Cys detection was proposed based on the *in situ* formation of a Bi_2MoO_6–Bi_2S_3 heterostructure on the indium–tin oxide (ITO) electrode. As illustrated in **Scheme 1**, Bi_2MoO_6 nanoparticles were initially coated on a bare ITO electrode. In the existence of L-Cys, Bi_2S_3 was generated *in situ* on the interface of Bi_2MoO_6/ITO by a chemical displacement reaction between sulfur ions from L-Cys and MoO_6^{6-} from Bi_2MoO_6. The compact contact and the matchable band-edge levels of Bi_2MoO_6 and Bi_2S_3 formed a heterostructure, which broadens the light absorption range and effectively restrains the electron–hole recombination, producing an improved photocurrent response. The increased concentrations of L-Cys could generate more amount of Bi_2S_3 on the Bi_2MoO_6/ITO interface, thereby boosting the photocurrent response. By this means, a signal-increased PEC system to quantitatively detect L-Cys was established by measuring the photocurrent change of the photoelectrode.

EXPERIMENTAL

Chemicals and Reagents

Bismuth nitrate ($Bi(NO_3)_3{\cdot}5H_2O$), ethylene glycol (EG), and sodium molybdate ($Na_2MoO_4{\cdot}2H_2O$) were purchased from Macklin Biochemical Co., Ltd. (Shanghai, China). L-Serine (L-Ser), glycine (Gly), and L-tyrosine (L-Tyr) were purchased from Sinopharm Chemical Reagent Co., Ltd. (China). L-Cys and glutathione (GSH) were obtained from Aladdin Reagent Inc. (Shanghai, China). Ascorbic acid (AA), sodium sulfate (Na_2SO_4), and sodium sulfite (Na_2SO_3) were purchased from Sinopharm Chemical Reagent Co., Ltd. (China). Phosphate buffer solution of 0.01 M (PBS, pH 7.4) was prepared with $NaH_2PO_4.2H_2O$, $K_2HPO_4.3H_2O$, and KCl. All chemical reagents were of analytical grade, and all aqueous solutions were prepared with ultrapure water (18.2 MΩ cm).

Apparatus

The PEC system consists of a CHI660E electrochemical workstation (Shanghai Chenhua Apparatus Corporation, China) and a PEAC 200A PEC reaction instrument (Tianjin Aidahengsheng Science-Technology Development Co., Ltd., China). PEC experiments and linear sweep voltammetry (LSV) curves were conducted on the PEC system using a three-electrode system: an ITO electrode with a geometric area of 0.25 cm^2 as the working electrode, a saturated Ag/AgCl electrode as the reference electrode, and a Pt wire as the counter electrode. The electrochemical impedance spectra (EIS) were implemented on a CHI660E electrochemical workstation in 5.0 mM K_3 $[Fe(CN)_6]$/K_4 $[Fe(CN)_6]$ solution containing 0.1 M KCl. The scanning electron microscope (SEM) images were acquired from the Hitachi S-4800 SEM (Tokyo, Japan). UV-visible diffuse reflection spectra were recorded using a PerkinElmer Lambda 950 UV-visible spectrophotometer (United States). X-ray photoelectron spectroscopy (XPS) images were recorded on a K-Alpha X-ray photoelectron spectrometer (Thermo Fisher Scientific Co., Waltham, MA, United States). Fourier transform infrared (FT-IR) spectra were acquired from the Bruker TENZOR 27 spectrophotometer (Bruker Optics, Germany).

Synthesis of Bi_2MoO_6 Nanoparticles

Bi_2MoO_6 was synthesized by a hydrothermal method (Dai et al., 2018). First, 0.4210 g of $Na_2MoO_4{\cdot}2H_2O$ was dissolved in 5 ml of EG under stirring for 0.5 h, and 1.6866 g of $Bi(NO_3)_3{\cdot}5H_2O$ solution was prepared in the same way. After mixing them together, 20 ml of ethanol was added dropwise under stirring. Second, the resulted solution was transferred into the Teflon-lined stainless steel

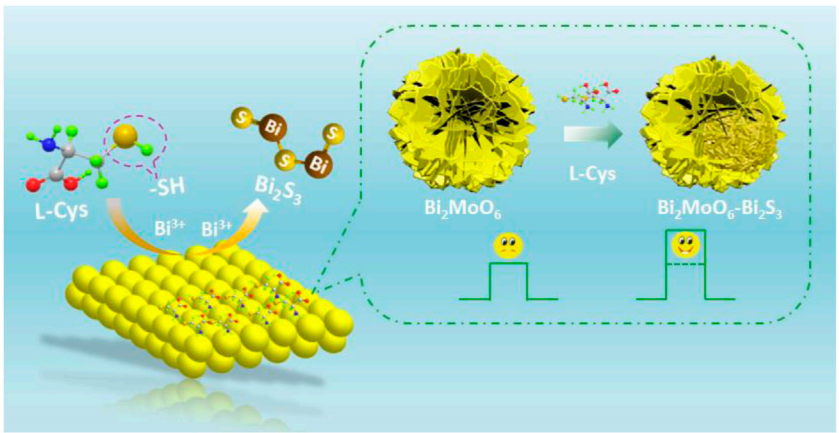

SCHEME 1 | Illustration of the proposed PEC sensor.

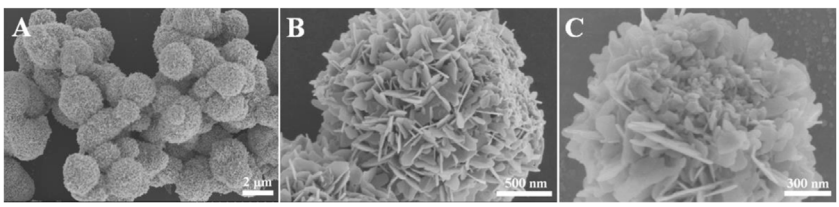

FIGURE 1 | SEM images of Bi_2MoO_6 **(A,B)** and Bi_2MoO_6 after reacting with L-Cys **(C)**.

autoclave, heated to 160°C for 12 h, and cooled to room temperature. Finally, the resultant product collected by centrifugation was washed three times with ethanol as well as water, dried overnight at 80°C, and then annealed at 400°C for 3 h to obtain Bi_2MoO_6 nanoparticles.

Fabrication of the Photoelectrochemical Biosensor

Bi_2MoO_6 suspension of 20 microliters with a concentration of 3 mg ml^{-1} was evenly dropped onto the cleaned ITO electrode and dried at 60°C for 20 min. Afterward, 20 μL of L-Cys solution was cast onto the surface of Bi_2MoO_6/ITO gently. After the reaction at 37°C for 0.5 h, the electrode was washed with water and then immersed in 0.01 M PBS (pH 7.4) containing 0.1 M AA for PEC measurement.

RESULTS AND DISCUSSION

Material Characterization

The morphology of Bi_2MoO_6 was characterized using the SEM. **Figures 1A,B** depicted that Bi_2MoO_6 possessed a nanosheet-assembled spherical structure, and the diameters of the microsphere were less than 3 μm. The stacked sheet structure makes the material have a large specific surface area, which benefits for the subsequent ion exchange reaction and the PEC detection. After incubated with L-Cys, parts of nanosheets granulated on the microsphere of Bi_2MoO_6 (**Figure 1C**), indicating the interaction between Bi_2MoO_6 and L-Cys. Additionally, the elemental mapping images in **Supplementary Figure S1** suggested that Bi, Mo, O, and S elements existed in the material, indicating the reaction between Bi_2MoO_6 and L-Cys.

To characterize the chemical composition and chemical state of Bi_2MoO_6 before and after reacting with L-Cys, XPS analysis was performed. As shown in **Figure 2A**, the elements of Bi, Mo, and O exist in Bi_2MoO_6 samples, whereas a new element of sulfur appeared after the reaction between Bi_2MoO_6 and L-Cys. Peaks in Bi 4f spectra in **Figure 2B** showed that two main peaks at 159.0 and 164.3 eV belong to Bi $4f_{5/2}$ and Bi $4f_{7/2}$ in Bi_2MoO_6 (Jia et al., 2018), shifted to 159.3 and 164.6 eV after the chemical reaction. This chemical shift originated from the formation of new bonds between bismuth and sulfur which changed the original chemical environment of bismuth atoms. The high-resolution XPS spectra of Mo 3d, S 2p, and O 1s of Bi_2MoO_6 after reacting with L-Cys were also conducted. The binding energy at 232.3, 235.4, 159.2, 164.4, and 531.1 eV pictured in **Figures 2C–E** were ascribed to Mo $3d_{5/2}$, Mo $3d_{3/2}$, S $2p_{3/2}$, S $2p_{1/2}$, and O 1 s, respectively. The result further witnessed the *in situ* formation of Bi_2S_3 on Bi_2MoO_6 (Li et al., 2020).

The optical property of Bi_2MoO_6 before and after reacting with L-Cys was studied by FT-IR spectroscopy and UV-vis DRS. As can be seen from **Figure 3A**, the characteristic peak at 712 cm^{-1} existed both in the FT-IR spectrum of Bi_2MoO_6 and

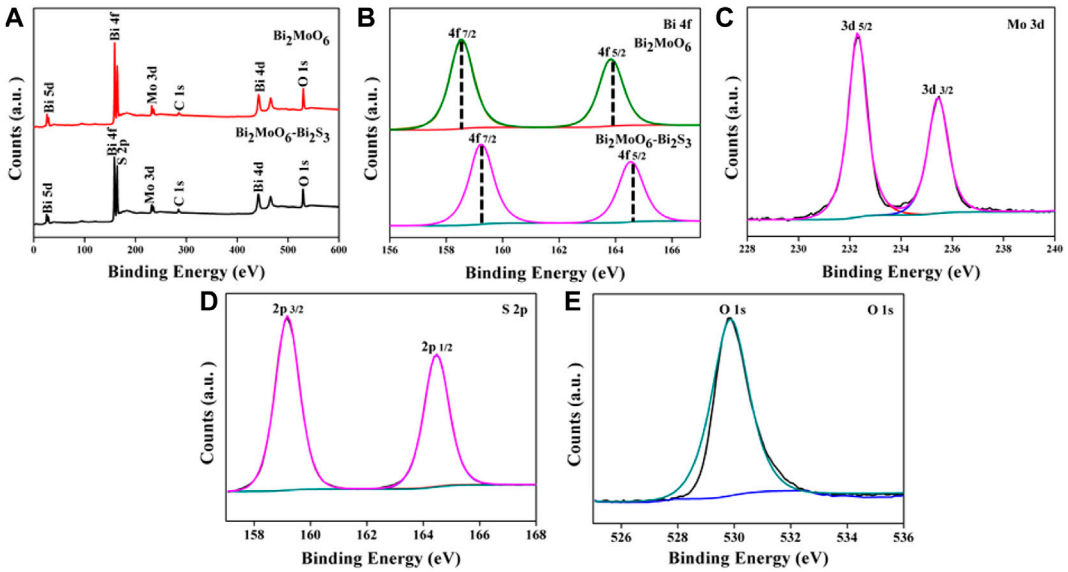

FIGURE 2 | XPS survey spectra of Bi_2MoO_6 before and after reacting with L-Cys **(A)**; high-resolution XPS spectra of Bi 4f **(B)**, Mo 3d **(C)**, S 2p **(D)**, and O 1s **(E)**.

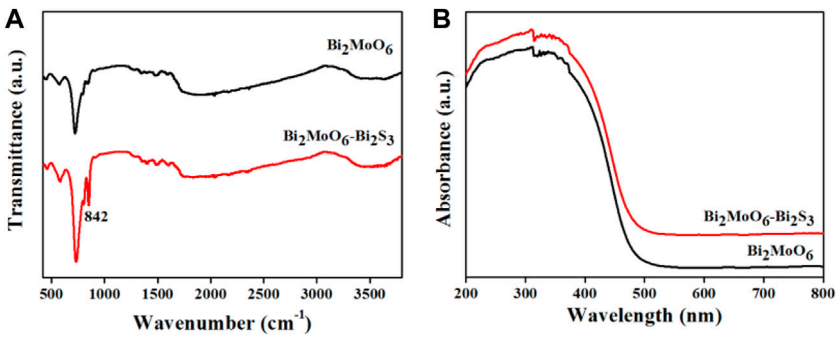

FIGURE 3 | FT-IR spectra of Bi_2MoO_6 and Bi_2MoO_6–Bi_2S_3 **(A)**; UV-vis DRS of Bi_2MoO_6 and Bi_2MoO_6–Bi_2S_3 **(B)**.

that after reacting with L-Cys, attributing to the symmetrical tensile vibration of the top oxygen atom of MoO_6^{6-} (Zhang et al., 2010; Li et al., 2014a; Tian et al., 2015). Compared with the FT-IR spectrum of Bi_2MoO_6, a new peak at 842 cm^{-1} appeared in the chart of Bi_2MoO_6 after the reaction with L-Cys. This new peak corresponds to the stretching vibration of Bi–S, indicative of the formation of Bi_2S_3 through the reaction between Bi_2MoO_6 and L-Cys (Zhao et al., 2017). The UV-vis DRS in **Figure 3B** suggested that the formation of Bi_2MoO_6–Bi_2S_3 widened the absorption range of the light irradiation and thus is benefit for the subsequent PEC analysis.

Condition Optimizations

As a photoactive material to construct the photoelectrode, the concentration of Bi_2MoO_6 plays a crucial effect on the PEC performance of the sensor. The photocurrent signal of the Bi_2MoO_6/ITO electrode constructed with varied concentration of Bi_2MoO_6 was recorded, and the photocurrent response reached a maximum value when the concentration of Bi_2MoO_6 was 3 mg ml^{-1} (**Supplementary Figure S2**). So, 3 mg ml^{-1} Bi_2MoO_6 was used for the subsequent experiments. In addition, the reaction time of Bi_2MoO_6 with L-Cys was optimized. According to **Supplementary Figure S3**, the photocurrent response gradually enhanced with the increase of reaction time, but the signal tended to stabilize when the reaction time reached 30 min. Therefore, 30 min was used as the reaction time.

Electrochemical and Photoelectrochemical Characterizations

To explore the interfacial electrochemical behavior of the biosensor, EIS analysis was conducted. As seen from **Figure 4A**, the bared ITO electrode displayed a small electron-transfer resistance (R_{et}), whereas the Bi_2MoO_6/ITO electrode gave an increased R_{et} because the coating of the semiconductor impedes the electron transfer. After Bi_2MoO_6/ITO

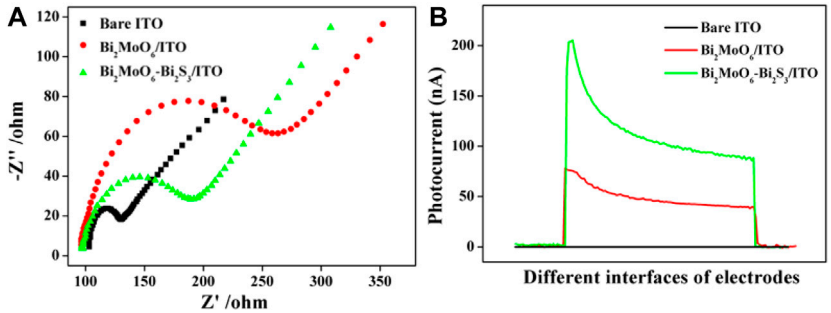

FIGURE 4 | EIS **(A)** and photocurrent intensity **(B)** of bare ITO, Bi_2MoO_6/ITO, and Bi_2MoO_6/ITO after reacting with L-Cys.

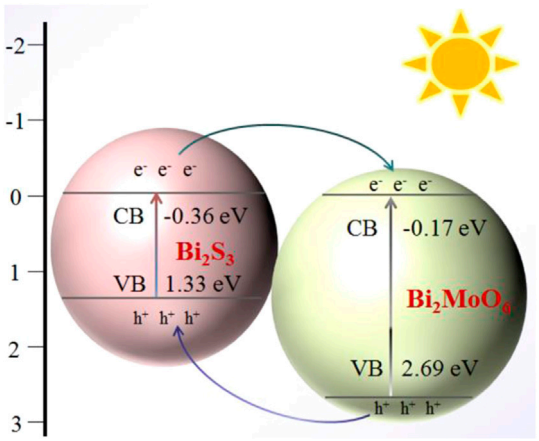

SCHEME 2 | Charge transfer of Bi_2MoO_6–Bi_2S_3 under visible light irradiation.

was incubated with L-Cys, the R_{et} declined. This result may be because the *in situ* formation of Bi_2S_3 on the interface of Bi_2MoO_6/ITO improved the electrical conductivity of the electrode. The photocurrent responses of the sensor at different modification stages were also investigated. As illustrated in **Figure 4B**, almost no PEC response was shown on the bare ITO electrode, while an evident photocurrent response was observed when Bi_2MoO_6 was immobilized on the electrode. After reacting with L-Cys (10 μmol L^{-1}), the Bi_2MoO_6/ITO electrode gave a much stronger photocurrent response. This is because the compact heterostructure formed between Bi_2S_3 and Bi_2MoO_6 by *in situ* formation of Bi_2S_3 on Bi_2MoO_6 and the matchable band-edge levels of Bi_2MoO_6 and Bi_2S_3 could effectively accelerate the transfer of the photo-excited charge carriers. The valence band (VB) and conduction band (CB) energy levels of Bi_2MoO_6 and Bi_2S_3 were determined by the electrochemical method (**Supplementary Figure S4**), and the charge transfer in Bi_2MoO_6–Bi_2S_3 heterostructure is illustrated in **Scheme 2**. Under the light irradiation, the photo-generated electrons in the CB of Bi_2S_3 (−0.36 eV) easily transferred to the CB of Bi_2MoO_6 (−0.17 eV), whereas the holes in the VB of Bi_2MoO_6 (2.69 eV) moved to the VB of Bi_2S_3 (1.33 eV).

Analytical Performance

The PEC response of the Bi_2MoO_6/ITO electrode toward L-Cys was explored. As depicted in **Figure 5A**, the photocurrent intensity enhanced along with the increase in L-Cys concentration. The reason of this variation trend may be that more L-Cys increased the amount of Bi_2S_3 *in situ* formed on the Bi_2MoO_6/ITO electrode, thus facilitating the charge transfer and boosting the photocurrent enhancement. As demonstrated in **Figure 5B**, the photocurrent intensity of the sensor showed a linear relationship with the logarithm of L-Cys concentrations when the concentrations varied in the range of 5.0×10^{-11}–1.0×10^{-4} mol L^{-1}. The linear equation is $I = 128.7 + 8.1 \log C_{L\text{-}Cys}$ ($R^2 = 0.997$). The limit of detection is 5.0×10^{-12} mol L^{-1}. Compared with some reported methods, this method demonstrates high detection sensitivity and a wide linear range for L-Cys (**Table 1**). The excellent performance of the sensor can be attributed to the *in situ* formation of Bi_2MoO_6–Bi_2S_3 heterostructure, which possesses an excellent photoelectric response under light irradiation.

Selectivity, Reproducibility, and Stability

The selectivity of the sensor was evaluated by testing the PEC response of Bi_2MoO_6/ITO toward Gly, L-Tyr, L-Lys, GSH, L-Ser, SO_3^{2-}, and SO_4^{2-} and the mixture of the aforementioned substances with L-Cys (all the aforementioned solutions have a concentration of 5 μmol L^{-1}). As pictured in **Figure 6A**, the PEC responses of Bi_2MoO_6/ITO to Gly, L-Tyr, L-Lys, GSH, and L-Ser showed no obvious change compared with the blank solution, whereas the response of L-Cys as well as the mixture of the aforementioned interferents with L-Cys exhibited an obvious enhancement, thus demonstrating good selectivity. The reproducibility of the sensor was studied by intra-assay and inter-assay of 10 μmol L^{-1} L-Cys. The relative standard deviations (RSDs) of intra-assay by using five Bi_2MoO_6/ITO electrodes in the same batch and inter-assay of the electrodes in different batches were 3.0 and 4.2%, respectively, indicating good reproducibility of the sensor. In addition, the photocurrent response of Bi_2MoO_6/ITO for 100 nmol L^{-1} L-Cys within 4 weeks of storage was investigated to study the stability of the sensor. As shown in **Figure 6B**, the photocurrents show negligible change with RSDs less than 5.1%. The signal of this system for 15 cycles was monitored. In **Supplementary Figure S5**, the photocurrent

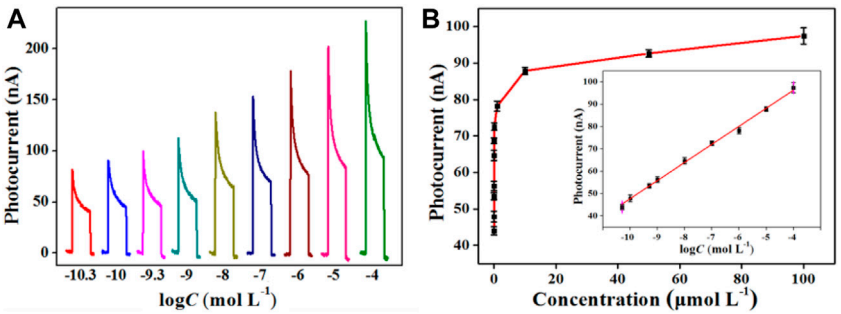

FIGURE 5 | Photocurrent responses of Bi_2MoO_6/ITO corresponding to L-Cys with varied concentrations **(A)**; relationship between photocurrent changes and L-Cys concentrations **(B)**; insert of part B, calibration curve between photocurrents and the logarithm of the L-Cys concentrations.

TABLE 1 | Comparison between this method and the reported methods for L-Cys detection.

Method	Material	Linear range (mol L^{-1})	LOD (mol L^{-1})	Reference
Amperometry	Y_2O_3NPs/N-rGO	1.3×10^{-6}–7.2×10^{-4}	8.0×10^{-7}	Yang et al. (2016)
Fluorescence	Carbon dots	0.0–3.0×10^{-5}	3.4×10^{-10}	Zong et al. (2014)
Colorimetry	CuNPs	0.0–2.5×10^{-5}	1.0×10^{-7}	Ahmed et al. (2016)
Electrochemiluminescence	PtNPs–RubRMs	1.0×10^{-9}–5.0×10^{-4}	3.3×10^{-10}	Wu et al. (2019)
Ratiometric absorption	AuNPs–CS/PLNPs-IBA	1.0×10^{-8}–5.5×10^{-6}	2.2×10^{-9}	Li et al. (2018)
Chronoamperometry	PB–AuNPs–Pd	3.0×10^{-7}–4.0×10^{-4}	1.8×10^{-7}	Pandey et al. (2012)
Cyclic voltammetry	PPy/GQDs@PB	2.0×10^{-7}–1.0×10^{-3}	1.50×10^{-7}	Wang et al. (2016)
PEC	Cu_2SnS_3@SnS_2	1.0×10^{-10}–3.0×10^{-4} 1.0×10^{-8}–1.0×10^{-4}	6.8×10^{-11} 8.5×10^{-9}	Wang et al. (2020)
PEC	Bi_2MoO_6	5.0×10^{-11}–1.0×10^{-4}	5.0×10^{-12}	This work

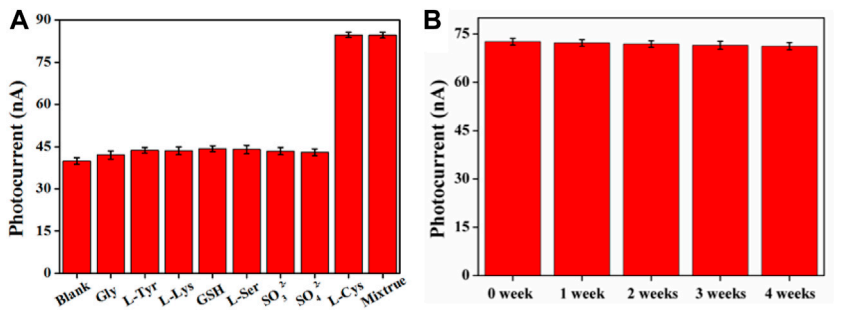

FIGURE 6 | Selectivity **(A)** and stability **(B)** of the PEC sensor.

was stable with a RSD of 3.2%. The data indicate the good stability of the sensor.

Applications

To explore the practical application of the sensor, seven undiluted human serum samples from Xinyang Central Hospital were measured. As listed in **Supplementary Table S1**, compared with the reference method (enzymatic cycling) used by the hospital, the relative errors between the reference method and this method are less than 6.1%, and the RSDs are no more than 6.2%. In addition, the standard addition test results suggest that the recoveries of L-Cys are in the range of 90.0–110.0% with RSDs less than 6.8%, as shown in **Supplementary Table S2**. The aforementioned results show that this method has good accuracy and feasibility.

CONCLUSION

In summary, a facile and signal-increased PEC sensor for L-Cys detection was developed based on the *in situ* formation of Bi_2MoO_6–Bi_2S_3 heterostructure. In virtue of the chemical reaction between L-Cys and Bi_2MoO_6, Bi_2S_3 was formed *in situ*

on the surface of Bi_2MoO_6, and the signal-increased sensing system endowed the sensor with high sensitivity. The Bi_2MoO_6–Bi_2S_3 heterostructure showed effective photoelectric conversion efficiency and thus demonstrated sensitive photocurrent response under light irradiation. Thanks to the fine performance of the Bi_2MoO_6–Bi_2S_3 heterostructure, the sensor for L-Cys achieved excellent performance in sensitivity, selectivity, and stability. The proposed method based on the *in situ* growth reaction not only proposes a new strategy for L-Cys detection but also opens up a new perspective for PEC bioanalysis.

DATA AVAILABILITY STATEMENT

The original contributions presented in the study are included in the article/**Supplementary Material**; further inquiries can be directed to the corresponding authors.

AUTHOR CONTRIBUTIONS

H-JX: conceptualization, methodology, investigation, and writing–original draft. X-JL: investigation. HW: investigation. S-WR: validation. J-TC: conceptualization, methodology, project administration, writing–original draft, and writing–review and editing. Y-ML: conceptualization, methodology, supervision, project administration, writing–original draft, and writing–review and editing.

FUNDING

This work was supported by the National Natural Science Foundation of China (Grant Nos. 21874115 and 21675136), Zhongyuan Thousand Talents Program of Henan Province (Nos. ZYQR201912127 and ZYQR201912177), Key Scientific Research Project of Higher Education Institutions in Henan Province (No. 22A150022), and Nanhu Young Scholar Supporting Program of XYNU.

SUPPLEMENTARY MATERIAL

The Supplementary Material for this article can be found online at: https://www.frontiersin.org/articles/10.3389/fchem.2022.845617/full#supplementary-material

REFERENCES

Ayaz Ahmed, K. B., Sengan, M., P., S. K., and Veerappan, A. (2016). Highly Selective Colorimetric Cysteine Sensor Based on the Formation of Cysteine Layer on Copper Nanoparticles. *Sensors Actuators B: Chem.* 233 (10), 431–437. doi:10.1016/j.snb.2016.04.125

Cao, J.-T., Lv, J.-L., Liao, X.-J., Ma, S.-H., and Liu, Y.-M. (2021). Photogenerated Hole-Induced Chemical-Chemical Redox Cycling Strategy on a Direct Z-Scheme Bi_2S_3/Bi_2MoO_6 Heterostructure Photoelectrode: Toward an Ultrasensitive Photoelectrochemical Immunoassay. *Anal. Chem.* 93 (28), 9920–9926. doi:10.1021/acs.analchem.1c02175

Chen, L., He, J., Liu, Y., Chen, P., Au, C.-T., and Yin, S.-F. (2016). Recent Advances in Bismuth-Containing Photocatalysts with Heterojunctions. *Chin. J. Catal.* 37 (6), 780–791. doi:10.1016/S1872-2067(15)61061-0

Dai, W., Hu, X., Wang, T., Xiong, W., Luo, X., and Zou, J. (2018). Hierarchical CeO_2/Bi_2MoO_6 Heterostructured Nanocomposites for Photoreduction of CO_2 into Hydrocarbons under Visible Light Irradiation. *Appl. Surf. Sci.* 434, 481–491. doi:10.1016/j.apsusc.2017.10.207

Deáková, Z., Ďuračková, Z., Armstrong, D. W., and Lehotay, J. (2015). Two-Dimensional High Performance Liquid Chromatography for Determination of Homocysteine, Methionine and Cysteine Enantiomers in Human Serum. *J. Chromatogr. A* 1408, 118–124. doi:10.1016/j.chroma.2015.07.009

Dong, Y.-X., Cao, J.-T., Wang, B., Ma, S.-H., and Liu, Y.-M. (2017). Exciton-Plasmon Interactions Between CdS@g-C_3N_4 Heterojunction and Au@Ag Nanoparticles Coupled with DNAase-Triggered Signal Amplification: Toward Highly Sensitive Photoelectrochemical Bioanalysis of MicroRNA. *ACS Sustain. Chem. Eng.* 5 (11), 10840–10848. doi:10.1021/acssuschemeng.7b02774

Hou, T., Zhang, L., Sun, X., and Li, F. (2016). Biphasic Photoelectrochemical Sensing Strategy Based on *In Situ* Formation of CdS Quantum Dots for Highly Sensitive Detection of Acetylcholinesterase Activity and Inhibition. *Biosens. Bioelectron.* 75, 359–364. doi:10.1016/j.bios.2015.08.063

Huang, Z., Yang, Y., Long, Y., and Zheng, H. (2018). A Colorimetric Method for Cysteine Determination Based on the Peroxidase-Like Activity of Ficin. *Anal. Methods* 10 (54), 2676–2680. doi:10.1039/C8AY00707A

Jia, Y., Ma, Y., Tang, J., and Shi, W. (2018). Hierarchical Nanosheet-Based Bi_2MoO_6 Microboxes for Efficient Photocatalytic Performance. *Dalton Trans.* 47 (16), 5542–5547. doi:10.1039/C8DT00061A

Laura Betti, L. P., Betti, L., and Giannaccini, G. (2015). Sulfur Metabolism and Sulfur-Containing Amino Acids: I-Molecular Effectors. *Biochem. Pharmacol. (Los Angel)* 04 (7), 1–8. doi:10.4172/2167-0501.1000158

Li, H., Liu, J., Hou, W., Du, N., Zhang, R., and Tao, X. (2014a). Synthesis and Characterization of G-C_3N_4/Bi_2MoO_6 Heterojunctions with Enhanced Visible Light Photocatalytic Activity. *Appl. Catal. B: Environ.* 160-161, 89–97. doi:10.1016/j.apcatb.2014.05.019

Li, J.-J., Qiao, D., Zhao, J., Weng, G.-J., Zhu, J., and Zhao, J.-W. (2019). Fluorescence Turn-On Sensing of L-Cysteine Based on FRET Between Au-Ag Nanoclusters and Au Nanorods. *Spectrochimica Acta A: Mol. Biomol. Spectrosc.* 217, 247–255. doi:10.1016/j.saa.2019.03.092

Li, J., Yang, C., Wang, W.-L., and Yan, X.-P. (2018). Functionalized Gold and Persistent Luminescence Nanoparticle-Based Ratiometric Absorption and TR-FRET Nanoplatform for High-Throughput Sequential Detection of L-Cysteine and Insulin. *Nanoscale* 10 (31), 14931–14937. doi:10.1039/C8NR04414G

Li, R., Yan, R., Bao, J., Tu, W., and Dai, Z. (2016). A Localized Surface Plasmon Resonance-Enhanced Photoelectrochemical Biosensing Strategy for Highly Sensitive and Scatheless Cell Assay Under Red Light Excitation. *Chem. Commun.* 52 (79), 11799–11802. doi:10.1039/C6CC05964C

Li, R., Zhang, Y., Tu, W., and Dai, Z. (2017). Photoelectrochemical Bioanalysis Platform for Cells Monitoring Based on Dual Signal Amplification Using *In Situ* Generation of Electron Acceptor Coupled with Heterojunction. *ACS Appl. Mater. Inter.* 9 (27), 22289–22297. doi:10.1021/acsami.7b06107

Li, W., Xie, P., Chen, J., He, J., Guo, X., Yu, D., et al. (2014b). Quantitative Liquid Chromatography-Tandem Mass Spectrometry Method for Determination of Microcystin-RR and its Glutathione and Cysteine Conjugates in Fish Plasma and Bile. *J. Chromatogr. B* 963, 113–118. doi:10.1016/j.jchromb.2014.05.057

Li, X., Chen, D., Li, N., Xu, Q., Li, H., He, J., et al. (2020). Efficient Reduction of Cr(VI) by a BMO/Bi_2S_3 Heterojunction via Synergistic Adsorption and Photocatalysis Under Visible Light. *J. Hazard. Mater.* 400, 123243. doi:10.1016/j.jhazmat.2020.123243

Liao, X.-J., Xiao, H.-J., Cao, J.-T., Ren, S.-W., and Liu, Y.-M. (2021). A Novel Split-Type Photoelectrochemical Immunosensor Based on Chemical Redox Cycling Amplification for Sensitive Detection of Cardiac Troponin I. *Talanta* 233, 122564. doi:10.1016/j.talanta.2021.122564

Lv, J.-L., Wang, B., Liao, X.-J., Ren, S.-W., Cao, J.-T., and Liu, Y.-M. (2021). Chemical-Chemical Redox Cycling Amplification Strategy in a Self-Powered Photoelectrochemical System: A Proof of Concept for Signal Amplified

Photocathodic Immunoassay. *Chem. Commun.* 57 (15), 1883–1886. doi:10.1039/D0CC08240F

Ma, Z.-Y., Xu, F., Qin, Y., Zhao, W.-W., Xu, J.-J., and Chen, H.-Y. (2016). Invoking Direct Exciton-Plasmon Interactions by Catalytic Ag Deposition on Au Nanoparticles: Photoelectrochemical Bioanalysis with High Efficiency. *Anal. Chem.* 88 (8), 4183–4187. doi:10.1021/acs.analchem.6b00503

Meng, L., Xiao, K., Zhang, X., Du, C., and Chen, J. (2020). A Novel Signal-Off Photoelectrochemical Biosensor for M.SssI MTase Activity Assay Based on GQDs@ZIF-8 Polyhedra as Signal Quencher. *Biosens. Bioelectron.* 150, 111861. doi:10.1016/j.bios.2019.111861

Pandey, P. C., Pandey, A. K., and Chauhan, D. S. (2012). Nanocomposite of Prussian Blue Based Sensor for L-Cysteine: Synergetic Effect of Nanostructured Gold and Palladium on Electrocatalysis. *Electrochimica Acta* 74, 23–31. doi:10.1016/j.electacta.2012.03.179

Peng, J., Huang, Q., Liu, Y., Huang, Y., Zhang, C., and Xiang, G. (2020). Photoelectrochemical Detection of L-Cysteine with a Covalently Grafted ZnTAPc-Gr-based Probe. *Electroanalysis* 32 (6), 1237–1242. doi:10.1002/elan.201900505

Qiu, Z., Shu, J., and Tang, D. (2018). Plasmonic Resonance Enhanced Photoelectrochemical Aptasensors Based on g-C_3N_4/Bi_2MoO_6. *Chem. Commun.* 54 (52), 7199–7202. doi:10.1039/C8CC04211J

Qiu, Z., and Tang, D. (2020). Nanostructure-Based Photoelectrochemical Sensing Platforms for Biomedical Applications. *J. Mater. Chem. B* 8 (13), 2541–2561. doi:10.1039/C9TB02844G

Song, N., Zhu, Y., Ma, F., Wang, C., and Lu, X. (2018). Facile Preparation of Prussian Blue/Polypyrrole Hybrid Nanofibers as Robust Peroxidase Mimics for Colorimetric Detection of L-Cysteine. *Mater. Chem. Front.* 2 (4), 768–774. doi:10.1039/C7QM00571G

Tian, J., Hao, P., Wei, N., Cui, H., and Liu, H. (2015). 3D Bi_2MoO_6 Nanosheet/TiO_2 Nanobelt Heterostructure: Enhanced Photocatalytic Activities and Photoelectochemistry Performance. *ACS Catal.* 5 (8), 4530–4536. doi:10.1021/acscatal.5b00560

Wang, B., Xu, Y.-T., Lv, J.-L., Xue, T.-Y., Ren, S.-W., Cao, J.-T., et al. (2019a). $Ru(NH_3)_6^{3+}$/$Ru(NH_3)_6^{2+}$-Mediated Redox Cycling: Toward Enhanced Triple Signal Amplification for Photoelectrochemical Immunoassay. *Anal. Chem.* 91 (6), 3768–3772. doi:10.1021/acs.analchem.8b05129

Wang, H., Yuan, F., Wu, X., Dong, Y., and Wang, G.-L. (2019b). Enzymatic *In Situ* Generation of Covalently Conjugated Electron Acceptor of PbSe Quantum Dots for High Throughput and Versatile Photoelectrochemical Bioanalysis. *Analytica Chim. Acta* 1058, 1–8. doi:10.1016/j.aca.2019.01.057

Wang, H., Zhang, B., Xi, J., Zhao, F., and Zeng, B. (2019c). Z-Scheme I-BiOCl/CdS with Abundant Oxygen Vacancies as Highly Effective Cathodic Material for Photocathodic Immunoassay. *Biosens. Bioelectron.* 141, 111443. doi:10.1016/j.bios.2019.111443

Wang, L., Liu, Z., Wang, D., Ni, S., Han, D., Wang, W., et al. (2017). Tailoring Heterostructured Bi_2MoO_6/Bi_2S_3 Nanobelts for Highly Selective Photoelectrochemical Analysis of Gallic Acid at Drug Level. *Biosens. Bioelectron.* 94, 107–114. doi:10.1016/j.bios.2017.02.045

Wang, L., Tricard, S., Yue, P., Zhao, J., Fang, J., and Shen, W. (2016). Polypyrrole and Graphene Quantum Dots @ Prussian Blue Hybrid Film on Graphite Felt Electrodes: Application for Amperometric Determination of L-cysteine. *Biosens. Bioelectron.* 77, 1112–1118. doi:10.1016/j.bios.2015.10.088

Wang, Q., Zhou, M., and Zhang, L. (2020). A Dual Mode Photoelectrochemical Sensor for Nitrobenzene and L-Cysteine Based on 3D Flower-Like Cu_2SnS_3@SnS_2 Double Interfacial Heterojunction Photoelectrode. *J. Hazard. Mater.* 382, 121026. doi:10.1016/j.jhazmat.2019.121026

Wu, J., Ran, P., Zhu, S., Mo, F., Wang, C., and Fu, Y. (2019). A Highly Sensitive Electrochemiluminescence Sensor for the Detection of L-Cysteine Based on the Rhombus-Shaped Rubrene Microsheets and Platinum Nanoparticles. *Sensors Actuators B: Chem.* 278, 97–102. doi:10.1016/j.snb.2018.09.066

Wu, L.-L., Wang, L.-Y., Xie, Z.-J., Pan, N., and Peng, C.-F. (2016). Colorimetric Assay of L-Cysteine Based on Peroxidase-Mimicking DNA-Ag/Pt Nanoclusters. *Sensors Actuators B: Chem.* 235, 110–116. doi:10.1016/j.snb.2016.05.069

Wu, Y., Song, M., Wang, Q., Wang, T., and Wang, X. (2018). A Highly Selective Conversion of Toxic Nitrobenzene to Nontoxic Aminobenzene by Cu_2O/Bi/Bi_2MoO_6. *Dalton Trans.* 47 (26), 8794–8800. doi:10.1039/C8DT01536H

Yang, S., Li, G., Wang, Y., Wang, G., and Qu, L. (2016). Amperometric L-Cysteine Sensor Based on a Carbon Paste Electrode Modified with Y_2O_3 Nanoparticles Supported on Nitrogen-Doped Reduced Graphene Oxide. *Microchim. Acta* 183 (4), 1351–1357. doi:10.1007/s00604-015-1737-8

Yu, S.-Y., Mei, L.-P., Xu, Y.-T., Xue, T.-Y., Fan, G.-C., Han, D.-M., et al. (2019a). Liposome-Mediated *In Situ* Formation of AgI/Ag/BiOI Z-Scheme Heterojunction on Foamed Nickel Electrode: A Proof-Of-Concept Study for Cathodic Liposomal Photoelectrochemical Bioanalysis. *Anal. Chem.* 91 (6), 3800–3804. doi:10.1021/acs.analchem.9b00352

Yu, S.-Y., Zhang, L., Zhu, L.-B., Gao, Y., Fan, G.-C., Han, D.-M., et al. (2019b). Bismuth-Containing Semiconductors for Photoelectrochemical Sensing and Biosensing. *Coord. Chem. Rev.* 393, 9–20. doi:10.1016/j.ccr.2019.05.008

Zhang, L., Luo, Z., Zeng, R., Zhou, Q., and Tang, D. (2019). All-Solid-State Metal-Mediated Z-Scheme Photoelectrochemical Immunoassay with Enhanced Photoexcited Charge-Separation for Monitoring of Prostate-Specific Antigen. *Biosens. Bioelectron.* 134, 1–7. doi:10.1016/j.bios.2019.03.052

Zhang, L., Xu, T., Zhao, X., and Zhu, Y. (2010). Controllable Synthesis of Bi_2MoO_6 and Effect of Morphology and Variation in Local Structure on Photocatalytic Activities. *Appl. Catal. B: Environ.* 98 (3–4), 138–146. doi:10.1016/j.apcatb.2010.05.022

Zhao, G., Zhang, D., Yu, J., Xie, Y., Hu, W., and Jiao, F. (2017). Multi-Walled Carbon Nanotubes Modified Bi_2S_3 Microspheres for Enhanced Photocatalytic Decomposition Efficiency. *Ceramics Int.* 43 (17), 15080–15088. doi:10.1016/j.ceramint.2017.08.036

Zhou, Q., Lin, Y., Lu, M., and Tang, D. (2017). Bismuth Ferrite-Based Photoactive Materials for the Photoelectrochemical Detection of Disease Biomarkers Coupled with Multifunctional Mesoporous Silica Nanoparticles. *J. Mater. Chem. B* 5 (48), 9600–9607. doi:10.1039/C7TB02354E

Zhu, J.-H., Feng, Y.-G., Wang, A.-J., Mei, L.-P., Luo, X., and Feng, J.-J. (2021). A Signal-On Photoelectrochemical Aptasensor for Chloramphenicol Assay Based on 3D Self-Supporting AgI/Ag/BiOI Z-Scheme Heterojunction Arrays. *Biosens. Bioelectron.* 181, 113158. doi:10.1016/j.bios.2021.113158

Zhu, Y., Xu, Z., Yan, K., Zhao, H., and Zhang, J. (2017). One-Step Synthesis of CuO-Cu_2O Heterojunction by Flame Spray Pyrolysis for Cathodic Photoelectrochemical Sensing of L-Cysteine. *ACS Appl. Mater. Inter.* 9 (46), 40452–40460. doi:10.1021/acsami.7b13020

Zong, J., Yang, X., Trinchi, A., Hardin, S., and Cole, I. (2014). Carbon Dots as Fluorescent Probes for "Off-On" Detection of Cu^{2+} and L-Cysteine in Aqueous Solution. *Biosens. Bioelectron.* 51, 330–335. doi:10.1016/j.bios.2013.07.042

Conflict of Interest: The authors declare that the research was conducted in the absence of any commercial or financial relationships that could be construed as a potential conflict of interest.

Publisher's Note: All claims expressed in this article are solely those of the authors and do not necessarily represent those of their affiliated organizations, or those of the publisher, the editors, and the reviewers. Any product that may be evaluated in this article, or claim that may be made by its manufacturer, is not guaranteed or endorsed by the publisher.